

# Persistence of the first-order transition lines in mesoscopic $\text{Bi}_2\text{Sr}_2\text{CaCu}_2\text{O}_8$ vortex matter with less than hundred vortices

M. Konczykowski,<sup>1</sup> Y. Fasano\*,<sup>2</sup> M.I. Dolz,<sup>3</sup> H. Pastoriza,<sup>2</sup> V. Mosser,<sup>4</sup> and M. Li<sup>5</sup>

<sup>1</sup>Laboratoire des Solides Irradiés, Ecole Polytechnique, CNRS URA-1380, 91128 Palaiseau, France

<sup>2</sup>Laboratorio de Bajas Temperaturas, Centro Atómico Bariloche, 8400 Bariloche, Argentina

<sup>3</sup>Departamento de Física, Universidad de San Luis, 5700 San Luis, Argentina

<sup>4</sup>Iron SAS, F-92448 Issy-les-Moulineaux, France

<sup>5</sup>Kamerlingh Onnes Laboratorium, Rijksuniversiteit Leiden, 2300 RA Leiden, The Netherlands

(Dated: March 22, 2022)

The persistence of the first-order transition line in the phase diagram of *mesoscopic*  $\text{Bi}_2\text{Sr}_2\text{CaCu}_2\text{O}_8$  vortex matter is detected down to a system size of less than hundred vortices. Precise and highly-sensitive to bulk currents *AC* magnetization techniques proved to be mandatory in order to obtain this information. The location of the vortex matter first-order transition lines are not altered by decreasing the sample size down to  $20\ \mu\text{m}$ . Nevertheless, the onset of irreversible magnetization is affected by increasing the sample surface-to-volume ratio producing a noticeable enlargement of the irreversible vortex region above the second-peak transition.

PACS numbers: 74.25.Uv, 74.25.Ha, 74.25.Dw

## I. INTRODUCTION

The vortex matter phase diagram in macroscopic samples of clean layered high-temperature superconductors presents a first-order transition (FOT) line<sup>1,2</sup> between a solid phase at low fields and temperatures and a liquid<sup>3</sup> or decoupled gas<sup>4</sup> of pancake vortices with reduced shear viscosity<sup>5</sup>. At low temperatures the solid phase presents irreversible magnetic behavior ascribed to bulk pinning and surface barriers, each of them dominating at different temperature and measuring-time ranges<sup>6-8</sup>. Direct imaging of the low-field phase in pristine samples of the extremely anisotropic  $\text{Bi}_2\text{Sr}_2\text{CaCu}_2\text{O}_8$  compound reveals a vortex solid with quasi long-range positional order<sup>9,10</sup>. Heavy-ion-irradiated  $\text{Bi}_2\text{Sr}_2\text{CaCu}_2\text{O}_8$  samples also present a FOT at low fields though in this case the vortex solid is polycrystalline<sup>11,12</sup>. These findings indicate that the positional order of the solid phase is therefore not relevant for the order of the transition<sup>12</sup>. Josephson-plasma-resonance measurements reveal the FOT corresponds to a single-vortex decoupling process between stacks of pancake vortices in adjacent CuO planes<sup>13</sup>. Therefore, there is evidence that the first-order transition is actually a single-vortex transition that depends, at best, on the density of the surrounding vortex matter. This can be further tested by decreasing the sample size down to a few micrometers such that, at low fields, the system size is reduced to only a few vortices.

The FOT of vortex matter in  $\text{Bi}_2\text{Sr}_2\text{CaCu}_2\text{O}_8$  can be detected at high temperatures,  $0.66 T_c \lesssim T < T_c$ , as a jump in the local flux density, or, in some cases, in the reversible magnetization<sup>2</sup>, or, alternatively, by a frequency-independent paramagnetic peak in the in-phase component of the first-harmonic of the AC screening signal<sup>14</sup>. Both features develop at the same field, identified with the first-order transition field  $H_{\text{FOT}}$ . The irreversible magnetic response of the system in this high-temperature

regime is dominated by a surface barrier. Depending on the sample geometry, this barrier can be of the geometrical or Bean-Livingston type<sup>7,15</sup>, while the bulk of the sample remains magnetically reversible<sup>8</sup>. In the intermediate temperature region  $0.39 T_c \lesssim T \lesssim 0.66 T_c$ , bulk pinning increases its relevance on cooling and the paramagnetic peak is masked by bulk shielding currents, entailing a sudden decrease of the AC signal<sup>14</sup>. Finally, in the low-temperature regime  $T \lesssim 0.39 T_c = 35\ \text{K}$ , bulk pinning plays a dominant role and the so-called second-peak effect<sup>6,16</sup> or order-disorder transition<sup>17-19</sup> is detected. This transition is manifested as a local increase of the width of DC hysteresis loops<sup>6</sup>, and as a minimum in AC magnetization loops with the field-location of the feature,  $H_{\text{SP}}$ , being frequency-independent<sup>20,21</sup>.

The persistence of these transition lines when decreasing the sample size down to few vortices is still open to discussion. Whether the thermodynamic  $H_{\text{FOT}}$  transition remains in mesoscopic vortex matter consisting of only a few vortices has, to our knowledge, not yet been investigated. Regarding the  $H_{\text{SP}}$  transition, two works of the same authors have reported on its disappearance on decreasing the sample system size down to  $30\ \mu\text{m}$ <sup>22,23</sup>. The authors attributed this phenomenology to the sample size becoming smaller than the temperature-dependent Larkin-Ovchinnikov correlation length<sup>24</sup> down which the vortex structure is insensitive to the pinning potential. This interpretation is contradictory with their own data since they invoke bulk current arguments for a system that clearly presents a surface-barrier-dominated physics as deduced from the two-quadrant locus of their DC magnetization loops<sup>22,23</sup>. Other work reports on a sample-size-dependent  $H_{\text{SP}}$ , even when not extremely varying the millimeter-range sample size, attributed to a distribution of metastable disordered vortex states with different lifetimes<sup>25</sup>.

In this work we report on the phase-location of the  $H_{\text{FOT}}$ ,  $H_{\text{SP}}$ , and irreversibility,  $H_{\text{irr}}$ , lines for *macro-*

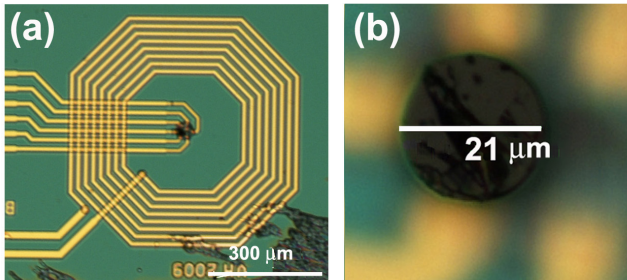


Figure 1: Optical microscope image of a  $21\ \mu\text{m}$  diameter  $\text{Bi}_2\text{Sr}_2\text{CaCu}_2\text{O}_8$  disk mounted on one of the on-chip Hall sensors embedded with the excitation coil. (a) Large scale view of the two adjacent 2D electron gas Hall sensors, with active areas of  $6 \times 6\ \mu\text{m}^2$ , and separated by  $20\ \mu\text{m}$ . The coil is used to generate a ripple AC field with frequencies up to 1 kHz. (b) Zoom of the sensor region with the disk placed on the left sensor. The surface of the sample is flat such as this results from cleaving; the observed heterogeneities on brightness are due to an irregular height of the Apiezon N grease used to glue the sample and to guarantee good thermal contact with the sensors chip.

*scopic* and *micron-sized*  $\text{Bi}_2\text{Sr}_2\text{CaCu}_2\text{O}_8$  single crystals, with the field applied parallel to the sample  $c$ -axis. We show that the  $H_{\text{FOT}}$  and  $H_{\text{SP}}$  transition fields do persist down to a system size of the order of hundred vortices. In addition, we reveal that these features present the same signature and location in the phase diagram, independently of decreasing the sample size down to  $21\ \mu\text{m}$ .

## II. EXPERIMENTAL

Single-crystals of optimally-doped  $\text{Bi}_2\text{Sr}_2\text{CaCu}_2\text{O}_8$  with  $T_c = 90\ \text{K}$  were grown by means of the traveling-solvent floating zone technique<sup>26</sup>. We selected two high-quality crystals from the same batch. The first one was taken as the reference  $220 \times 220 \times 30\ \mu\text{m}^2$  macroscopic crystal and the second one was used to engineer micron-sized disks. The latter are obtained by means of optical lithography of the sample surface and subsequent physical ion-milling in the disks' negative<sup>27</sup>. The resulting micron-sized towers are removed by cleaving the milled surface with a resist-wetted silicon substrate. The resist is then chemically eliminated. The resulting circular samples have typical thicknesses of  $1\ \mu\text{m}$  and diameters ranging from 10 to  $50\ \mu\text{m}$ . The disks are then mounted onto Hall-sensor chips with micron-precision manipulators, and glued with Apiezon N grease.

The local magnetization or, more precisely, the stray field, of the disks was measured with microfabricated 2D electron gas Hall sensors<sup>28</sup> with  $6 \times 6\ \mu\text{m}^2$  active surface embedded with an excitation coil on a single chip. Figure 1 shows a photograph of one of the studied disks mounted on one of two adjacent sensors. The remaining empty sensor is used as a local reference of the applied

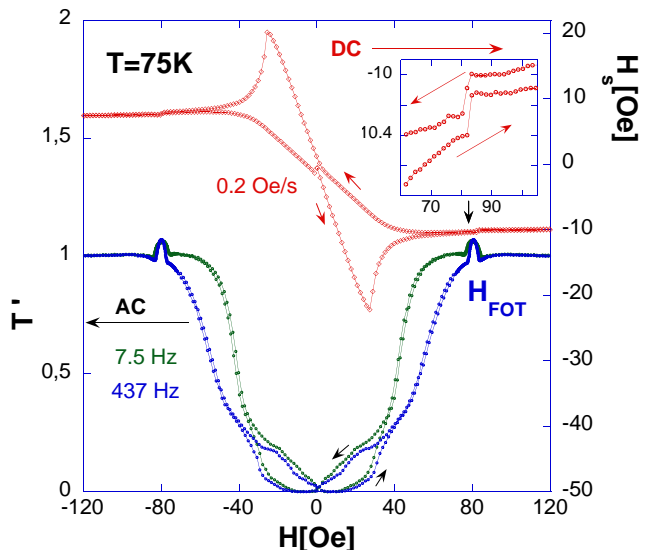


Figure 2: High-temperature DC and AC magnetic hysteresis loops of the reference  $\text{Bi}_2\text{Sr}_2\text{CaCu}_2\text{O}_8$  macroscopic crystal measured at  $75\ \text{K}$ . Top: ascending and descending branches of the DC hysteresis loop. Inset: zoom-in of the DC loop at the vicinity of the first-order transition entailing a  $B$ -jump (see black arrow). Red arrows indicate the ascending and descending branches. Bottom: AC transmittivity loops with paramagnetic peaks fingerprinting the first-order transition field  $H_{\text{FOT}}$ . The loops were measured with ripple fields of  $0.9\ \text{Oe}$  rms and frequencies of  $7.5$  and  $437\ \text{Hz}$ . Black arrows indicate the ascending and descending branches.

magnetic field when performing DC experiments. The macroscopic sample was measured by means of similar chips supporting several Hall sensors with active areas ranging from  $6 \times 6$  to  $40 \times 40\ \mu\text{m}^2$ . The Hall array is always placed over the center of the sample. The on-chip embedded coil generates an AC field parallel to the applied DC field  $H$ . In all the experiments presented here this ripple field has an amplitude of  $H_{\text{AC}} = 0.9\ \text{Oe}$  rms, while its frequency ranges from 1 to 1000 Hz. The current applied to the sensors is in the range of 25 to  $50\ \mu\text{A}$ . A digital-signal-processing lock-in technique is used to simultaneously measure the in- and out-of-phase components of the fundamental and the third-harmonic frequencies of the Hall voltage.

In this way, several DC and AC local magnetic measurements were performed using the same set-up, as a function of temperature, magnetic field, and frequency. The DC magnetic hysteresis loops are obtained by measuring the magnetization,  $H_S = B - H$ , when cycling the static applied field  $H$ . During the AC measurements, an  $H_{\text{AC}}$  field collinear to  $H$  is applied and the first- and third-harmonic of the AC response of Hall sensors is simultaneously recorded. The in-phase component of the first-harmonic signal  $B'$  is converted to the transmittivity  $T' = [B'(T) - B'(T \ll T_c)] / [B'(T > T_c) - B'(T \ll T_c)]$ <sup>29</sup>. This magnitude is more sensitive to discontinuities in the local induction than direct measurements of the static

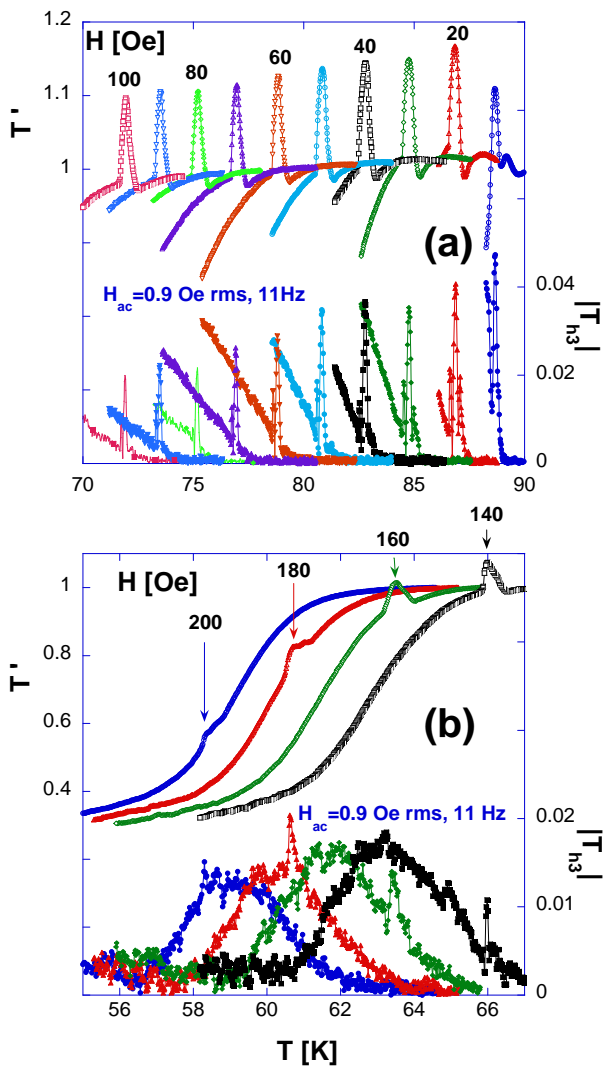


Figure 3: Temperature-dependence of the transmittivity and modulus of the third harmonic response for the reference  $\text{Bi}_2\text{Sr}_2\text{CaCu}_2\text{O}_8$  macroscopic crystal. (a) Low field and (b) high field regimes. The AC ripple field of 0.9 Oe rms and 11 Hz is collinear to the applied field  $H$ .

induction  $B$ . The modulus of the third harmonic signal  $|T_{h3}| = |B_{h3}^{\text{AC}}| / [B'(T > T_c) - B'(T \ll T_c)]$  becomes non negligible at the onset of irreversible magnetic properties (see Fig. 3). This onset is then used to track  $H_{\text{irr}}$ <sup>30</sup>.

We perform two types of measurements, temperature evolution of  $T'$  and  $|T_{h3}|$  on field-cooling in several fields, and isothermal DC and AC hysteresis loops<sup>31</sup> as, for instance, shown in Fig. 2. By means of the AC technique, the first-order transition field and the onset of magnetic irreversibility are detected with better resolution than by DC loop measurements. In the high-temperature regime, the FOT is manifest in the AC transmittivity as a prominent paramagnetic peak that develops at the same  $H$  as the jump in local induction detected in DC hysteresis loops<sup>14,31</sup>.

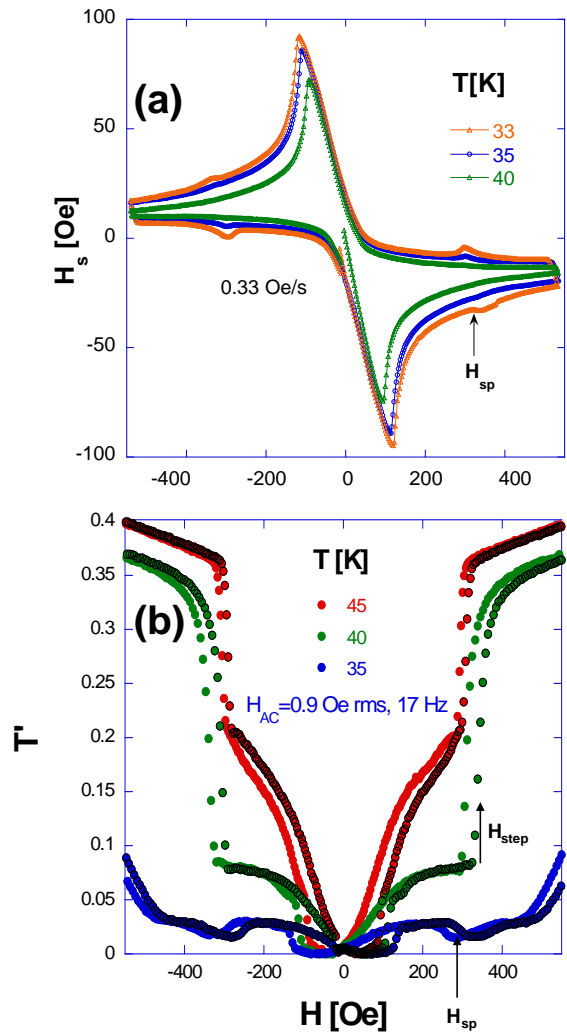


Figure 4: DC and AC magnetic hysteresis loops in the low-intermediate temperature regime for the  $\text{Bi}_2\text{Sr}_2\text{CaCu}_2\text{O}_8$  macroscopic crystal. (a) DC loops from which the transition field  $H_{\text{SP}}$  is taken at the midpoint between the onset and the full development of the local minimum in the ascending branch (see arrow). (b) Transmittivity AC loop measured with a ripple field of 0.9 Oe rms and 17 Hz parallel to  $H$ . At each temperature, black-on-color points correspond to the positive ascending and negative descending field branches of the transmittivity curve. The  $H_{\text{SP}}$  field is obtained similarly as in DC loops (see arrow). The field location of the step-like feature,  $H_{\text{step}}$ , is taken at half the step height in the ascending field branch (see arrow).

### III. RESULTS

#### A. Reference macroscopic sample

The magnetic properties of the reference macroscopic  $\text{Bi}_2\text{Sr}_2\text{CaCu}_2\text{O}_8$  sample present three characteristic temperature regimes. Figure 2 depicts the magnetic hysteretic response of the reference macroscopic sample at

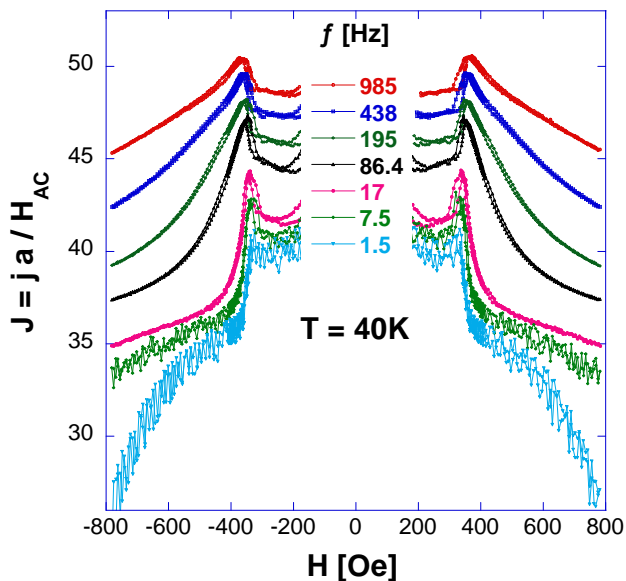


Figure 5: Normalized sustainable-current density  $J$  as a function of applied field at 40 K for the  $\text{Bi}_2\text{Sr}_2\text{CaCu}_2\text{O}_8$  macroscopic crystal. The frequency dependence of  $J$  is obtained from AC magnetization loops measured with a ripple field of 0.9 Oe rms and frequencies ranging 1.5 to 985 Hz.

high-temperature,  $T = 0.83 T_c$ . The top panel shows a two-quadrant DC loop such as typically obtained in this temperature regime. Closer inspection of the DC data in the vicinity of 80 Oe reveals a  $H_S$  jump with similar height for both, ascending and descending branches. This feature is the fingerprint of the first-order transition  $H_{\text{FOT}}$  in the high-temperature region. The bottom panel of Fig. 2 shows that, in AC loops, this transition is detected with improved resolution: paramagnetic peaks emerge at the flanks of the central  $T'$  depletion<sup>31</sup>. On increasing frequency, the system enhances its shielding capability manifested as a  $T'$  decrease. The field-location of the paramagnetic peak in AC loops is frequency-independent, and is therefore considered as  $H_{\text{FOT}}$ .

Figure 3 shows a set of AC magnetic data for low applied fields ranging from 10 to 200 Oe. The paramagnetic peak in  $T'$  shifts towards lower temperatures on increasing field. The peaks are sharp and all transmittivity curves have the same high-temperature background up to 100 Oe. On cooling at higher fields, shielding currents develop in the sample prior to the appearance of the paramagnetic peak. Nevertheless, Fig. 3 (b) shows that the paramagnetic peaks can be detected up to 200 Oe. The irreversibility line, identified from the onset of the third-harmonic signal on cooling, is located at temperatures higher than the paramagnetic peak. This indicates the existence of a phase region with non-linear vortex dynamics at fields exceeding  $H_{\text{FOT}}$ <sup>32</sup>. The amplitude of  $|T_{\text{h3}}|$  decreases on increasing the applied field, see Fig. 3 (b). In addition, the  $|T_{\text{h3}}|$  curve echoes the paramagnetic peak in  $T'$ .

The  $H_{\text{SP}}$  transition field can be obtained from DC magnetic hysteresis loops as those shown in Fig. 4 (a) for low-intermediate temperatures. In these curves the local minimum (maximum) of the ascending (descending) branch becomes more evident on cooling. The loops occupy two field-quadrants and noticeably increase their width on cooling. This figure also indicates that the  $H_{\text{SP}}$  field is hard to detected from DC magnetic loops for temperatures higher than 33 K. This is due to a technical limitation of the DC technique that lacks resolution in order to measure bulk transitions in the high-temperature regime where surface barriers dominate the magnetic properties<sup>7</sup>.

We therefore use the AC hysteresis loop technique in order to track the first-order transition up to higher temperatures. The AC transmittivity reflects the dimensionless normalized sustainable-current density,  $J = j(f)a/H_{\text{AC}}$ , provided  $J = (1/\pi) \arccos(2T' - 1)$ <sup>30</sup>. This formula was derived for an AC penetration in the Bean critical regime, an assumption that seems to be valid in view of the results presented in Ref. 32. A low-temperature AC loop at 35 K is shown in Fig. 4 (b) depicting local minima in both, the ascending and descending branches. These minima can be ascribed to the second-peak transition  $H_{\text{SP}}$  since a minimum in  $T'$  corresponds to a maximum in the bulk  $J$ . The  $T'$  signal evolves in a different manner for the high- and intermediate-temperature regimes. For temperatures larger than  $0.66 T_c = 58$  K, the transmittivity presents paramagnetic peaks, developing at the flanks of the central depletion (see Fig. 2). For intermediate temperatures a sudden jump of  $T'$  is detected, as for instance in the AC loops measured at 40 and 45 K. This step-like feature, manifested at a field  $H_{\text{step}}$  implies a frequency-independent drop of the magnetic hysteresis, consistent with the change in the width of the DC loops, and indicating that this transition is governed by the local value of  $B$  rather than  $H$ <sup>33</sup>. The jump in  $T'$  is related to the sudden change in shielding currents with the sample becoming more transparent to the penetration of the AC ripple field at larger  $H$ . Similarly, the height of the steps in  $T'$  decreases on increasing temperature.

The crossover temperature for the detection of the second-peak or of the step-like feature is time/frequency dependent. Figure 5 presents the evolution of the normalized sustainable-current density extracted from  $T'$  as a function of frequency in the range from 1.5 to 985 Hz. For frequencies smaller than 7.5 Hz a sudden drop of  $J$  develops at fields  $H_{\text{SP}} \sim 330$  Oe. On increasing frequency, this feature evolves into a field-asymmetric peak producing the step-like feature observed in  $T'$  curves. The onset of this peak, or equivalently the  $H_{\text{step}}$  field in  $T'$ , is frequency independent.

Finally, Fig. 6 presents the vortex matter phase diagram of the macroscopic  $\text{Bi}_2\text{Sr}_2\text{CaCu}_2\text{O}_8$  sample in the high-temperature region, indicating the  $H_{\text{FOT}}$  (full points) and the  $H_{\text{irr}}$  (open points) lines. Both lines merge for  $T > 70 \text{ K} = 0.77 T_c$ , whereas at smaller tem-

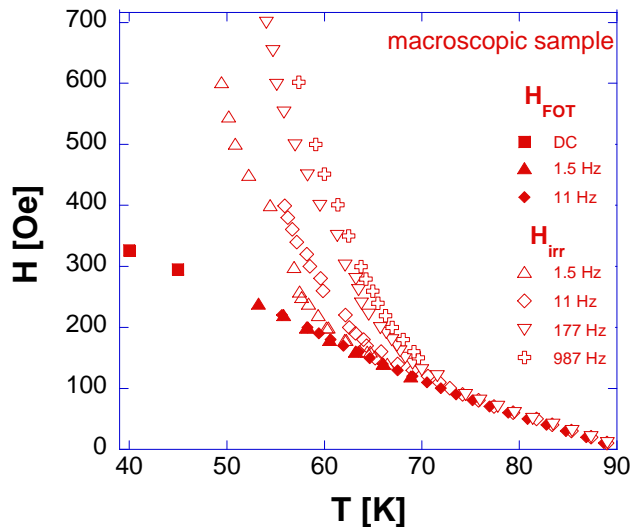


Figure 6: Vortex phase diagram of the macroscopic reference  $\text{Bi}_2\text{Sr}_2\text{CaCu}_2\text{O}_8$  sample. First-order transition (full points) and irreversibility (open points) lines from DC and AC magnetic measurements at different frequencies. At low temperatures, the  $H_{\text{irr}}$  line strongly depends on frequency. Measurements were performed at an AC ripple field of 0.9 Oe rms.

peratures, the  $H_{\text{irr}}$  line deviates towards higher fields and is strongly frequency-dependent. The higher the frequency, the larger is the deviation from the FOT line. The onset of  $|T_{\text{h}3}|$  indicates the electric field  $E = E(H_{\text{AC}}, f, J)$  becomes non-linear below a working point given by the experimental resolution. As temperature decreases, the linear response limit shrinks to smaller current-density values. Therefore, the onset of third harmonic response shifts to lower temperatures for smaller frequencies (smaller currents).

### B. Micron-sized samples

As discussed in the previous section, performing AC measurements is necessary in order to properly track the FOT line, particularly in the case of samples of highly-reduced size in which surface barriers for vortex flux entry/exit completely dominate the electromagnetic response. The insert to Fig. 7 shows the transmittivity data for the  $21 \mu\text{m}$  diameter disk at the smallest measurement field of 5 Oe. The paramagnetic peak fingerprinting the  $H_{\text{FOT}}$  is clearly visible for this system consisting of only 80 vortices. Tracking the location in the temperature-field plane of this peak yields the first-order transition line in the vortex phase diagram shown in the main panel of Fig. 7. An important finding of this figure is the persistence of the  $H_{\text{FOT}}$  transition line for micron-sized vortex matter from  $T_c$  down to  $75 \text{ K} = 0.83 T_c$ . The first-order transition line is also detected down to

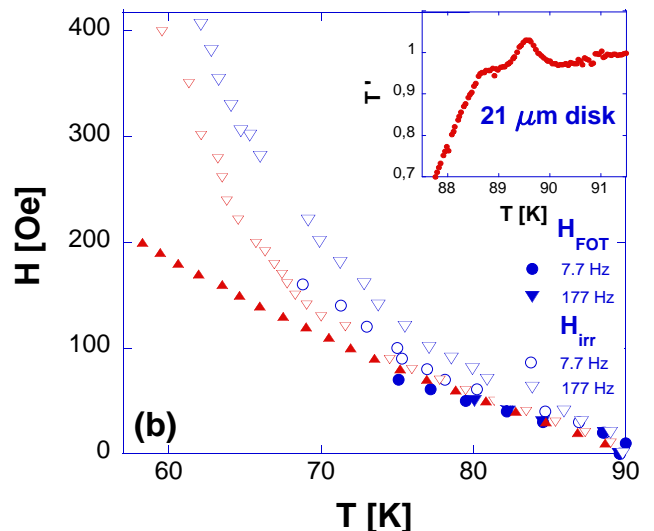


Figure 7: Vortex phase diagram of micron-sized  $\text{Bi}_2\text{Sr}_2\text{CaCu}_2\text{O}_8$  vortex matter for the smallest measured disk of  $21 \mu\text{m}$  diameter (blue points). First-order transition (full points) and irreversibility (open points) lines. Data from the macroscopic reference sample (red points) are included for comparison. Inset: Low-field transmittivity for the smallest measured field of 5 Oe. Measurements were performed at an AC ripple field of 0.9 Oe rms and 7.7 and 177 Hz.

similar temperatures in larger disks. This indicates that, even for samples with a large surface-to-volume ratio, the  $H_{\text{FOT}}$  transition measured at high-temperatures remains robust. For  $T < 75 \text{ K}$  no paramagnetic peak is detected in the transmittivity data, presumably due to a masking effect produced by enhanced surface barriers in small samples. The  $H_{\text{FOT}}$  line for the disks merges that of the macroscopic reference sample, indicating that the nature of this transition does not change even for a system with just 80 vortices, for the smallest applied field of 5 Oe in the  $21 \mu\text{m}$  sample (see Fig. 7).

The  $H_{\text{irr}}$  line for micron-sized samples is located at higher fields than for the macroscopic sample. For example, Fig. 7 shows that at low temperatures  $H_{\text{irr}}$  is  $\sim 35\%$  larger for the  $21 \mu\text{m}$  disk than for the macroscopic sample at a fixed frequency (177 Hz in this case). This result might have origin in the different aspect ratio of the macroscopic and disk samples, and in their probably dissimilar surface roughness originating from the different preparation methods for both specimens. Ascertaining the origin of this discrepancy is beyond the aim of this paper. Figure 7 also shows that for smaller frequencies  $H_{\text{irr}}$  approaches the first-order transition line. Finally, in the high-temperature range the irreversibility lines for the macroscopic and micron-sized samples merge into a single bunch of data with the  $H_{\text{FOT}}$  line.

We also study the effect of decreasing the sample size down to microns on the  $H_{\text{SP}}$  transition. Previous works using DC magnetic techniques reported that this tran-

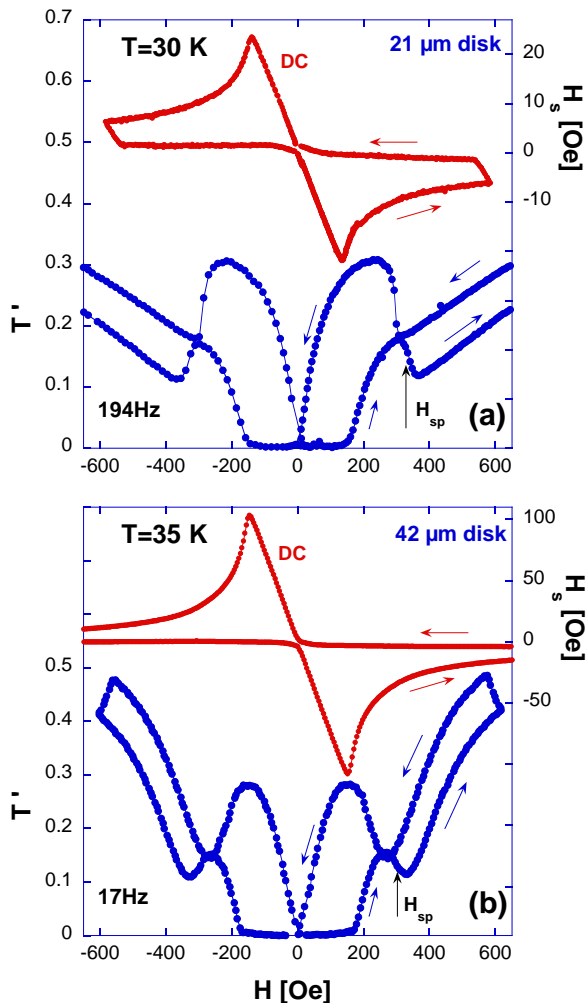


Figure 8: Low-temperature magnetic hysteresis loops for  $\text{Bi}_2\text{Sr}_2\text{CaCu}_2\text{O}_8$  micron-sized disks for DC (top red curves) and AC (bottom blue curves) measurements: (a) smallest  $21\ \mu\text{m}$  diameter measured disk at 30 K and (b)  $42\ \mu\text{m}$  diameter disk at 35 K. The ripple field is of 0.9 Oe rms and 194 Hz for the smaller disk and 17 Hz for the largest one. The transition field  $H_{\text{SP}}$  considered as the mid-point between the onset and the full development of the minimum in the ascending branch is indicated with an arrow.

sition field is not detected for samples with diameters smaller than  $30\ \mu\text{m}$ <sup>22,23</sup>. We performed AC measurements in order to study the persistence or absence of the  $H_{\text{SP}}$  transition. Fig. 8 shows the comparison of DC and AC loops data: while the DC loops do not show evidence of the  $H_{\text{SP}}$  feature, the local minima in the ascending and descending branches of the AC loops are evident. Even measuring at intermediate (194 Hz) and low (17 Hz) frequencies, the application of the AC technique enables the observation of the emergence of the bulk current contribution, therefore allowing the detection of  $H_{\text{SP}}$ . Figure 8 depicts a remarkably well-developed  $T'$  local minimum for the 21 and  $42\ \mu\text{m}$  diameter disks, giving a  $H_{\text{SP}}$  field

that is within 10% of the value observed in macroscopic samples (roughly 330 Oe).

Therefore, the results of Fig. 8 show that the previously reported absence of the  $H_{\text{SP}}$  transition for micron-sized disks of  $\text{Bi}_2\text{Sr}_2\text{CaCu}_2\text{O}_8$  is the consequence of a technical limitation. The mentioned works<sup>22,23</sup> apply DC magnetic techniques entailing large characteristic measurement times. In this case, surface currents play a determining role in screening, as already known from studies on macroscopic  $\text{Bi}_2\text{Sr}_2\text{CaCu}_2\text{O}_8$  crystals<sup>7</sup>.

#### IV. DISCUSSION

The three characteristic temperature regimes of the first-order phase transition of *macroscopic*  $\text{Bi}_2\text{Sr}_2\text{CaCu}_2\text{O}_8$  vortex matter are also found for *micron-sized* samples. In the latter case, the identification of the first-order transition is rendered more difficult by the enhancement of the surface to bulk-currents ratio. The nearly-vanishing remanent magnetization and the two-quadrant locus of the DC loops in *micron-sized* samples indicate the preeminence of surface barriers for vortex flux entry/exit. Therefore applying AC magnetic techniques is imperative in order to have access to the faster decaying bulk currents emerging from the surface-barrier background<sup>7</sup>.

In the intermediate- and low-temperature regimes  $T'$  and  $|T_{\text{h}3}|$  present particular features that are related to the bulk-current contribution. For  $0.39 T_c < T < 0.66 T_c$  we detect, at a field  $H_{\text{step}}$ , a discontinuous decrease of the bulk shielding-currents associated with the first-order transition. On cooling below  $T = 0.39 T_c = 35\ \text{K}$ , the opposite effect of an increase of the shielding currents is observed at almost the same field indicating the  $H_{\text{SP}}$  transition. In the vicinity of this reversal of current behavior, varying the frequency of the AC ripple field tunes a decrease (low-frequencies) or an increase (high-frequencies) of the shielding currents. The latter case is equivalent to probing magnetic relaxation on a shorter time-scale, in analogy to DC magnetization experiments<sup>7</sup>, or to choosing a higher electric field in an transport  $I(V)$  measurement. Since the  $I(V)$  curves just below and above the FOT cross — with the electric field in the high-field phase being larger than that in the low-field phase for the low-current density limit, and vice-versa for the high-current density limit —, varying the working point (by tuning the frequency) leads to either a step like-behavior of the screening current (at low electric fields) or a peak-like curve (at high electric fields)<sup>34</sup>. The energy barriers for flux creep have  $U(J)$  and  $E(J)$  curves with different functionalities for fields larger or smaller than the transition one. On varying field close to the transition these curves cross, and the phase transition produces a discontinuous change on the electrodynamics of vortex matter. Detecting the transition with a high electric field (short measurement times) leads to an enhancement of shielding currents with increasing field, whereas with a low electric

field (long times) a sudden decrease is observed. The lack of sensitivity of DC magnetization loops to the FOT in the intermediate-temperature regime can be understood as the consequence of a distribution of Bean-Livingston surface barriers<sup>15</sup>. The transit of individual pancake vortices over these barriers is not affected by the nature of the vortex phase inside the sample.

The irreversibility line obtained from the onset of  $|T_{h3}|$  merges with the first-order transition line  $H_{\text{FOT}}$  in the high-temperature regime. At lower temperatures or higher applied fields, the shielding of the AC field starts at higher temperatures than the occurrence of the first-order transition, namely, the onset of  $|T_{h3}|$  develops before the paramagnetic peak on cooling. This indicates the existence of a non-linear vortex region spanning at higher temperatures than the first-order transition line<sup>32</sup>. This phenomenon might have origin from a residual effect of pinning<sup>35</sup>, or Bean-Livingston barriers<sup>36</sup> on the high-temperature liquid phase. This phenomenology is observed in *macroscopic* as well as *micron-sized*  $\text{Bi}_2\text{Sr}_2\text{CaCu}_2\text{O}_8$  samples.

The most important finding of this work is that the first-order transition persists even for a very small vortex system. In the high-temperature regime, the clear detection of the paramagnetic peak at 5 Oe in the  $21\ \mu\text{m}$  disk is shown in the insert to Fig. 7. This result indicates that, independently of its nature, the first-order transition is robust and its thermodynamic nature remains unaltered even for a reduced system size of less than hundred vortices. In the low-temperature regime, the detection of the  $H_{\text{SP}}$  transition as a sudden increase of shielding currents (decrease of  $T'$ ) persists in *micron-sized* samples. The observation of this feature was made possible by the use of an AC magnetic measurement technique. The possibility of working at shorter time-scales (larger frequen-

cies) reveals currents flowing in the sample volume with improved sensitivity than DC measurements. Therefore, our results indicate that reducing the sample size down to few dozens of microns does not produce a disappearance nor a dramatic decrease of  $H_{\text{SP}}$  due to size effects as previously claimed<sup>22,23,25</sup>.

## V. CONCLUSIONS

In the high-temperature phase region, the first-order transition of  $\text{Bi}_2\text{Sr}_2\text{CaCu}_2\text{O}_8$  vortex matter remains robust and persists at the same  $H - T$  location even when decreasing the system size down to less than hundred vortices. We found that the second-peak transition detected in the low- and intermediate-temperature regions also persists on decreasing the system size down to roughly  $20\ \mu\text{m}$ , in contrast with previous reports<sup>22,23</sup>. The identification of these transitions increases in difficulty when decreasing the sample size, due to the predominance of surface-barrier-related currents. The application of AC magnetic techniques, with better sensitivity to bulk currents, allowed us to detect the transition-related features.

## VI. ACKNOWLEDGEMENTS

We thank C.J. van der Beek for selecting the crystals and discussing the manuscript. This work was supported by the ECOS Sud-MINCYT France-Argentina collaboration program, Grant No. A09E03. Work done at Bariloche was partially funded by PICT-PRH 2008-294 from the ANPCyT.

\* To whom correspondence should be addressed: yanina.fasano@cab.cnea.gov.ar

- 
- <sup>1</sup> H. Pastoriza and M. F. Goffman and A. Arribere and F. de la Cruz, Phys. Rev. Lett. **72**, 2951 (1994).
- <sup>2</sup> E. Zeldov and D. Majer and M. Konczykowski and V. B. Geshkenbein and V. M. Vinokur and H. Shtrikman, Nature **375**, 373 (1995).
- <sup>3</sup> D. R. Nelson, Phys. Rev. Lett. **60**, 1973 (1988).
- <sup>4</sup> L. I. Glazman and A. E. Koshelev, Phys. Rev. B **43**, 2835 (1991).
- <sup>5</sup> H. Pastoriza and P. H. Kes, Phys. Rev. Lett. **75**, 3525 (1995).
- <sup>6</sup> N. Chikumoto, M. Konczykowski, N. Motohira, K. Kishio, K. Kitazawa, Phys. C **185-189**, 2201 (1991).
- <sup>7</sup> N. Chikumoto, M. Konczykowski, N. Motohira, and A. P. Malozemoff, Phys. Rev. Lett. **69** 1260 (1992).
- <sup>8</sup> E. Zeldov, D. Majer, M. Konczykowski, A. I. Larkin, V. M. Vinokur, V. B. Geshkenbein, N. Chikumoto, and H. Shtrikman, Eur. Phys. Lett. **30**, 367 (1995).
- <sup>9</sup> Y. Fasano, M. De Seta, M. Menghini, H. Pastoriza and F. de la Cruz, Proc. Nat. Acad. Sciences **102**, 3898 (2005).
- <sup>10</sup> Y. Fasano, and M. Menghini, Supercond. Sc. and Tech. **21**, 023001 (2008).
- <sup>11</sup> S. S. Banerjee, Y. Myasoedov, E. Zeldov, M. Menghini, Y. Fasano, F. de la Cruz, C. J. van der Beek, M. Konczykowski, and T. Tamegai, Phys. Rev. Lett. **90**, 87004 (2003).
- <sup>12</sup> M. Menghini, Y. Fasano, F. de la Cruz, S. S. Banerjee, Y. Myasoedov, E. Zeldov, C. J. van der Beek, M. Konczykowski, and T. Tamegai, Phys. Rev. Lett. **90**, 147001 (2003).
- <sup>13</sup> S. Colson, M. Konczykowski, M. B. Gaifullin, Y. Matsuda, P. Gierlowski, M. Li, P. H. Kes, and C. J. van der Beek, Phys. Rev. Lett. **90**, 137002 (2003).
- <sup>14</sup> N. Morozov, E. Zeldov, D. Majer, and M. Konczykowski, Phys. Rev. B **54**, R3784 (1996).
- <sup>15</sup> N. Morozov, E. Zeldov, D. Majer and B. Khaykovich, Phys. Rev. Lett. **76** 138 (1996).
- <sup>16</sup> N. Avraham, B. Khaykovich, Y. Myasoedov, M. Rappaport, H. Shtrikman, D. E. Feldman, T. Tamegai, P. H. Kes, M. Li, M. Konczykowski, C. J. van der Beek, and E. Zeldov, Nature **411**, 451 (2001).
- <sup>17</sup> B. Khaykovich, M. Konczykowski, E. Zeldov, R. A. Doyle, D. Majer, P. H. Kes, and T. W. Li, Phys. Rev. B **56**, R517

- (1997).
- <sup>18</sup> V. M. Vinokur, B. Khaykovich, E. Zeldov, M. Konczykowski, R. A. Doyle, P. H. Kes, Phys. C **295**, 209 (1998).
- <sup>19</sup> R. Cubitt, E. M. Forgan, G. Yang, S. L. Lee, D. M. Paul, H. A. Mook, M. Yethiraj, P. H. Kes, T. W. Li, A. A. Menovsky, Z. Tarnawski, and K. Mortensen, Nature **365**, 407 (1993).
- <sup>20</sup> I. Sochnikov, A. Shaulov, and Y. Yeshurun, Journal App. Phys. **103** 07C705 (2008).
- <sup>21</sup> C.J. van der Beek, M.V. Indenbom, V. Berseth, T.W. Li, and W. Benoit, Journ. Low Temp. Phys. **105**, 1047 (1996).
- <sup>22</sup> Y. M. Wang, A. Zettl, T. Tamegai, and S. Ooi, Physica C **341**, 1109 (2000).
- <sup>23</sup> Y. M. Wang, M. S. Fuhrer, A. Zettl, S. Ooi, and T. Tamegai, Phys. Rev. Lett. **86** 3626 (2001).
- <sup>24</sup> A. I. Larkin and Yu. N. Ovchinnikov, J. Low. Temp. Phys. **34**, 409 (1979).
- <sup>25</sup> B. Kalisky, D. Giller, A. Shaulov, T. Tamegai, and Y. Yeshurun, Phys. Rev. B **72** 014531 (2005).
- <sup>26</sup> T. W. Li *et al.*, J. Cryst. Growth **135**, 481 (1994).
- <sup>27</sup> M. I. Dolz, A. B. Kolton and H. Pastoriza, Phy. Rev. B **81**, 092502 (2010).
- <sup>28</sup> M. Konczykowski, F. Holtzberg, and P. Lejay, Supercond. Sci. Technol. **4**, S331 (1991).
- <sup>29</sup> J. Gilchrist, and M. Konczykowski, Phys. C **212**, 43 (1993).
- <sup>30</sup> C. J. van der Beek, M. Konczykowski, V. M. Vinokur, G. W. Crabtree, T. W. Li, and P. H. Kes, Phys. Rev. B **51**, 15492 (1995).
- <sup>31</sup> M. Konczykowski, C. J. van der Beek, A. E. Koshelev, V. Mosser, M. Dogson, and P. H. Kes, Phys. Rev. Lett. **97**, 237005 (2006).
- <sup>32</sup> M. V. Indenbom, C. J. van der Beek, V. Berseth, M. Konczykowski, N. Motohira, H. Berger, W. Benoit, J. Low Temp. Phys. **105**, 1117 (1996).
- <sup>33</sup> B. Khaykovich, E. Zeldov, D. Majer, T. W. Li, P. H. Kes, and M. Konczykowski, Phys. Rev. Lett. **76**, 2555 (1996).
- <sup>34</sup> M. Konczykowski, S. Colson, C. J. van der Beek, M. V. Indenbom, P. H. Kes, and E. Zeldov, Phys. C **332** 219 (2000).
- <sup>35</sup> V. M. Vinokur, V. R. Geshkenbein, A. I. Larkin, and M. V. Feigelman, Zhurnal Eksperimentalnoi i Teoreticheskoi Fiziki **100**, 1104 (1991).
- <sup>36</sup> D. Fuchs, E. Zeldov, M. Rappaport, T. Tamegai, S. Ooi, and H. Shtrikman, Nature (London) **391**, 373 (1998).